Universidad Zaragoza
1542

Trabajo Fin de Máster
Máster en Ingeniería Biomédica

Cellular response due to substrate stiffness variations: A phenomenological model

Autor

Aarón Xerach Herrera Martín

Directores

José Manuel García Aznar
Carlos Borau Zamora

Departamento de Ingeniería Mecánica
Escuela de Ingeniería y Arquitectura
Universidad de Zaragoza

Septiembre 2013

Universidad Zaragoza
1542

Cellular response due to substrate stiffness variations: A phenomenological model

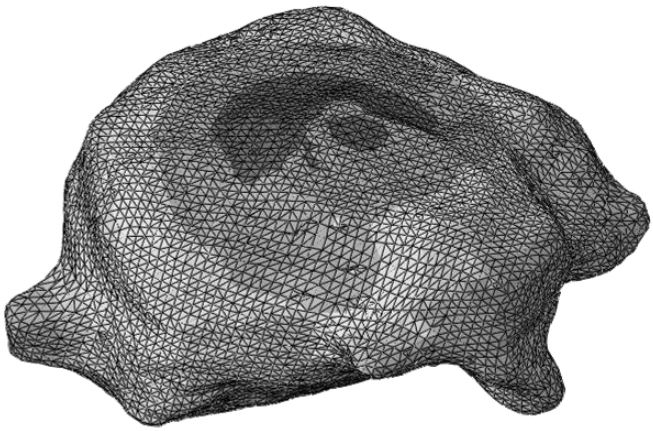

Main report

Main report

1. Introduction.

1.1. Cell migration and mechanosensing.

Cell migration plays a fundamental role in many physiological processes, such as morphogenesis, inflammatory response, immunological response, wound healing or cancer metastasis. An abnormal behaviour in cell migration can lead to different pathologies, so it becomes especially important to understand, for example, the cause by which cancer cells migrate from the initial tumour to the vascular system or what mechanisms leads the fibroblast and endothelial cells for wound healing.

In short, a better understanding of the cell migration process would permit the development of new therapies, increase the effectiveness of transplants or the efficiency of artificial tissues employed in regenerative surgery.

Cell migration can be described with five sequential stages that lead to cell movement:

- Front edge pseudopods protrusion.
- Focal adhesions formation.
- Focalized proteolysis.
- Cell contraction.
- Detachment and contraction of the cell rear edge.

The process starts with the protrusion of pseudopods in the front edge of the cell due to the pressure exerted by the actin filaments polymerizing and pushing on the cell membrane. These protrusions have an exploratory nature and appear in a semi-stochastic manner. Once the pseudopods are formed, integrins of the cell contact with the ligands of the extracellular matrix (ECM), gathering in the cell membrane and forming the focal adhesion whereby the pseudopods adhere to the substrate.

Then, enzymes of the cell degrade the substrate. After the proteolysis, the cell contraction proceeds due to the acto-myosin (AM) complex relative movement. While the cell is shrinking, focal adhesions of the rear edge detach from the substrate when stresses achieve a certain limit. In this way, the cell contracts and migrates through the ECM.

Cell behaviour is governed by different stimuli, which can be generally divided in three main groups: mechanics, topographic and chemical (Figure 1.1).

Cells are able to sense substrate stiffness (*mechanotaxis or durotaxis* [2]) or substrate deformation (*tensotaxis* [3]). In this regard, it has been demonstrated that cells tend to migrate to stiffer or more strained regions because focal adhesions are more stable, allowing exerting higher forces [4-6]. On the other hand, the cell response can be influenced by the concentration of chemical substances (*chemotaxis*) or non-soluble molecules (*haptotaxis*) [7]. Finally, topography can influence cell polarization and the cytoskeletal reorganization [8].

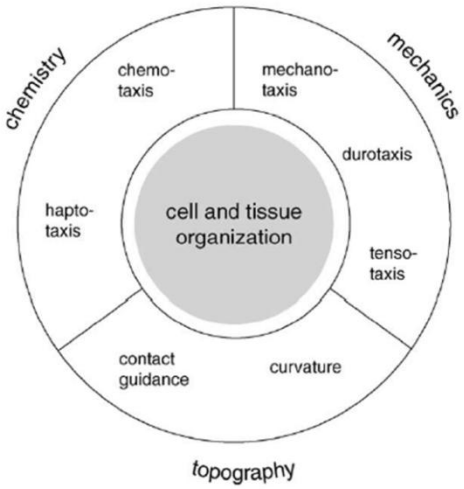

Figure 1.1. Main stimuli affecting cell migration [6].

As previously exposed, cells sense their environment conditions, determining not only migration-related phenomena but other significant processes. For instance, cell mechanosensing can lead to different cellular changes, such as membrane channel activity, altered cell morphology, alteration in protein synthesis because of changes in binding affinity, or gene expression due to force transmission to the nucleus and to the chromatin contained inside.

Although several factors take part in cell migration, this work is focused in the development of a cell contraction model depending on the mechanosensing mechanism that directly influences cell migration. The proper understanding of this process can establish the bases to a better knowledge of the whole problem and opening new research lines.

1.2. Previously developed cellular models.

There is a great variety of computational models that aims to study specific or general aspects of cell migration. All of them can be divided in three main groups depending on the studied area. These methods are explained below.

a) Cellular protrusion models.

Actin filaments polymerization against cell membrane is a basic aspect of cell migration. Single filament models have been developed, elucidating saturation forces and force-speed relationships. Generally, it is considered that the growing of the filament is due to actin monomers diffusion that tends to fill the holes generated by the Brownian movements of the cell membrane. These models allow studying the connection between the filaments and the membrane, establishing force-generation mechanisms that affect force-speed relationships [9-10].

Multiple filaments models study the interaction between the filaments and the crosslinking proteins, with special attention to the filopodia and lamellipodia protrusions by means of their polymerization a depolymerization [11-12]. Also there are continuous models to describe the actin lattice structure by means of the concentration and number of filaments in contact with the membrane, which allows them to study bigger systems.

These models allow obtaining actin domains, its concentration, force-speed relationships, lamellipodia speed protrusion, elastic and diffusive membrane properties or filament length distribution and orientation.

b) Adhesion-retraction models.

Since actin fibres cannot exert forces or movement without a mechanical union with the substrate, these types of models are crucial. Focal adhesion formation and cell-matrix interactions have been studied taking into account that applied forces have a direct effect in actin polymerization [13] or taking into account the interaction between these fibres and the integrins [14]. Also it has been studied the retraction of the rear edge of the cell, principally based on the myosin [15-16].

c) Whole cell models.

These models take into account dynamic and mechanic phenomenons, including molecular scale process, different detail levels and different time scales, approaching the cell mechanics as explicit or as phenomenological models. In addition, the models can be carried out by two main approximations: Migration of single cells [17-19] or collective [20-21].

Whole cell models can be studied from several different hypothesis: force based models, stochastic models, spheroids models and Monte Carlo studies. In the first one, cell migration is based on the force balance of the front and rear edge of the cell, as well as protrusion and drag forces due to the resistance exerted by the ECM [16]. Nevertheless, these models cannot predict migration of individual cells and do not take into account variations in cell shape or substrate properties owing to degradation. Stochastic models elucidate the movement of cell populations [22] but do not include factors as traction or drag forces, neither substrate properties. Cell spheroid models are based on pressure gradients produced by cell proliferation and death [23]. Combining stochastic movements, pressure and chemical activity of cellular aggregates, these models are appropriate for tumorous studies. However, these models do not include mechanical stimuli such as stiffness, density or matrix porosity. Finally, Monte Carlo studies use a set of simple rules that allows fast simulations, making them appropriate for long term cellular migratory patterns [1, 24].

1.3. Objectives.

As previously exposed, cells in organism respond to mechanical stimuli such as strains, forces, topography or ECM stiffness. An abnormal response to these stimuli is associated with several pathologies; therefore, numerous investigations have been developed to determinate cell behaviour and its interactions with the surrounding substrate.

Studies carried out by Mitrossilis et al. [1] demonstrate that force rate increases with substrate stiffness, in agreement with the Hill force-velocity relationship. Thus, cellular response can be considered similar to muscle adaptation to load, highlighting the role of the AM system as rigidity sensors, providing a mechanosensing mechanism through focal adhesions. In fact, this mechanism can translate anisotropy in the substrate

to anisotropy in the cytoskeleton, being able to modify focal adhesion formation and Ca^{2+} influx, increasing the AM contraction and leading the cell through stiffness gradients.

Due to the importance of how cells sense the mechanical properties of its surrounding substrate, this work aims to develop a three-dimensional computational model that allows reproducing the behaviour experimentally observed when a cell is placed between two plates of variable stiffness.

To reproduce this behaviour it is proposed a phenomenological model that includes a passive component simulating the cytoskeletal stiffness in parallel with an active component that simulates the behaviour of the AM complex. In this way, by coupling the stiffness dependent contraction of the AM system with the passive behaviour of the cell, the mechanosensing mechanism can be studied.

Finally, this model is used to study the behaviour of a real cell, whose geometry was obtained through confocal microscopy thanks to Ana Rozaut in the Centro de Investigación Médica Aplicada (CIMA) of Navarra University, allowing the observation of how tumorous cell deforms the surrounding ECM.

In sort, this work aims to develop a tool that allows elucidating the strains exerted by a cell when it is embedded in real three-dimensional substrates, and achieving a better understanding of the whole problem.

2. Phenomenological model of cellular response to substrate stiffness variations.

2.1. Material model.

2.1.1. 1-D approach.

The proposed model is based on the interaction between the cell and the ECM, without taking into account other factors like the interaction with other cells and chemical or biological factors that could influence its behaviour. Thus, the studied phenomenon is mechanically regulated by means of the relationship between the cell and substrate properties.

According to Buxboim et al. [26], cell exerts contractile forces to determine the substrate stiffness, stressing and straining it. In this way, the cytoskeleton adapts and polarizes according to the stress direction, creating new focal adhesions at the front edge and detaching the rear edge adhesions, which involves cell contraction and motility. Even though cytoskeletal adaptation and cell motility are different phenomena, both are led by cell mechanosensing.

The presented cellular model is based on a structure with two parallel springs and an actuator representing the main mechanical components of the cell:

- Actin filaments, simulated through a spring with K_{act} constant.
- AM contractile system, simulated through an actuator.
- Cell passive stiffness, due to microtubules, cytosol and cell membrane, initially simulated with a spring of K_{pas} constant.

Therefore, cell strain will depend on the imposed strain of the AM contractile system and the mechanical behaviour of the actin filaments and the cell passive stiffness. As previously exposed, the cellular cytoskeleton attaches to the substrate by mean of focal adhesions and trans-membrane integrins so, in a simplified manner and as first approach, this union is considered completely rigid.

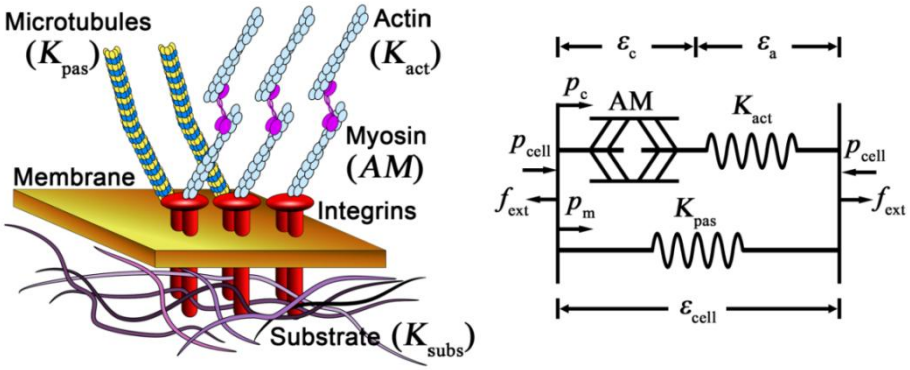

Figure 2.1. Schematic diagram of the components involved in cell contraction (left). Cellular contraction model with its components: Active side corresponding to $\boldsymbol{AM} + \boldsymbol{K_{act}}$ and the passive side corresponding to $\boldsymbol{K_{pas}}$ (right) [18].

The transmitted stress by the cell to the substrate ($\sigma_{cell,ij}$) depends on the cellular strain ($\varepsilon_{cell,ij}$). This strain can be divided in two sides: The actin filaments strain ($\varepsilon_{a,ij}$) and the AM complex strain ($\varepsilon_{c,ij}$), obtaining:

$$\varepsilon_{cell} = \varepsilon_c + \varepsilon_a \tag{2.1}$$

Since actin filaments are modelled with a linear elastic behaviour, its strain can be expressed as:

$$\varepsilon_a = \frac{p_c}{K_{act}} \tag{2.2}$$

Additionally, the stress exerted by the cell to the substrate corresponds to the sum of the AM complex stress and the stress absorbed by the passive components (K_{act} and K_{pas}):

$$p_{cell}(\varepsilon_{cell}) = p_c + p_m = p_c(\varepsilon_c) + K_{pas}\varepsilon_{cell} \tag{2.3}$$

Stress generated by the AM complex ($\sigma_{c,ii}$) is related with the overlap of their filaments [27]. Thus, according to Huxley's Law [28], it is assumed the following form:

$$p_c(\varepsilon_c) = \begin{cases} 0 & \varepsilon_c < \varepsilon_{min} \quad (1) \\ -\dfrac{p_{max}}{\varepsilon_{min}}\varepsilon_c + p_{max} & \varepsilon_{min} < \varepsilon_c < 0 \quad (2) \\ -\dfrac{p_{max}}{\varepsilon_{max}}\varepsilon_c + p_{max} & 0 < \varepsilon_c < \varepsilon_{max} \quad (3) \\ 0 & \varepsilon_{max} < \varepsilon_c \quad (4) \end{cases} \tag{2.4}$$

It can be distinguished four zones as function of the contractile side strain (ε_c), shown in figure 2.2. Under high compression loads (Zone 1: $\varepsilon_c < \varepsilon_{min}$), the AM complex cannot exert contraction. For reduced or zero load values, the mechanical equilibrium and the cell strain are led by the AM complex (Zone 2: $\varepsilon_{min} < \varepsilon_c < 0$). Under traction load cases (Zones 3 and 4) cell contraction is compensated, decreasing the contribution of the AM complex until ε_{max}, point from which it cannot exert any additional force.

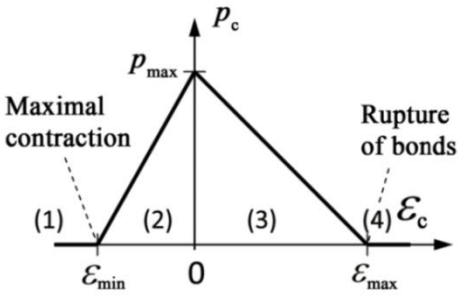

Figure 2.2. Exerted force by the AM complex as function of the filaments overlap. Zone 1: Passive behaviour. The AM complex is submitted to external compression loads. Zone 2: Contraction. The AM complex exerts force to sense the substrate properties. Zone 3: Traction. The AM is tractioned but it still presents contraction. Zone 4: Passive behaviour. The traction forces are too high, bonds break and no compression force is exerted by the AM complex [18].

Combining equations (2.1), (2.2) and (2.4) the following expressions can be obtained for each proposed zone:

$$\varepsilon_{cell} = \begin{cases} \dfrac{p_{cell}}{K_{pas}} & \varepsilon_c < \varepsilon_{min} \quad (1) \\ \varepsilon_c + \dfrac{\left(-\frac{p_{max}}{\varepsilon_{min}}\varepsilon_c + p_{max}\right)}{K_{act}} & \varepsilon_{min} < \varepsilon_c < \dfrac{p_{max}}{K_{act}} \quad (2) \\ \varepsilon_c + \dfrac{\left(-\frac{p_{max}}{\varepsilon_{max}}\varepsilon_c + p_{max}\right)}{K_{act}} & \dfrac{p_{max}}{K_{act}} < \varepsilon_c < \varepsilon_{max} \quad (3) \\ \dfrac{p_{cell}}{K_{pas}} & \varepsilon_{max} < \varepsilon_c \quad (4) \end{cases} \tag{2.5}$$

where the limits have been redefined because when the AM complex strain is null, it can be written as:

$$\varepsilon_{cell} = \varepsilon_a = \frac{p_{max}}{K_{act}} \tag{2.6}$$

Since the model control will be based on the active part, the expressions are reorganized as function of this side, obtaining:

$$\varepsilon_c = \begin{cases} \varepsilon_{cell} & \varepsilon_c < \varepsilon_{min} \quad (1) \\ \dfrac{\left(\varepsilon_{cell} - \dfrac{p_{max}}{K_{act}}\right)\varepsilon_{min}K_{act}}{\varepsilon_{min}K_{act} - p_{max}} & \varepsilon_{min} < \varepsilon_c < \dfrac{p_{max}}{K_{act}} \quad (2) \\ \dfrac{\left(\varepsilon_{cell} - \dfrac{p_{max}}{K_{act}}\right)\varepsilon_{max}K_{act}}{\varepsilon_{max}K_{act} - p_{max}} & \dfrac{p_{max}}{K_{act}} < \varepsilon_c < \varepsilon_{max} \quad (3) \\ \varepsilon_{cell} & \varepsilon_{max} < \varepsilon_c \quad (4) \end{cases} \tag{2.7}$$

2.1.2. 3-D model.

Since the model has been developed to be applied in three dimensional geometries, the equation 2.7 has been used independently for each direction of the 3D system (x,y,x) Thus, the contraction of the AM system in each direction directly depends on the cell strain in that direction ($\varepsilon_{c,w}(\varepsilon_{cell,w})$). Note that this formulation is only valid when the actin filaments are assumed to act as 1D components.

In any case, the model equations can be described for any kind of threedimensional behavior as follows:

$$\boldsymbol{\sigma_{cell}} = \boldsymbol{\sigma_c} + \boldsymbol{\sigma_p} \tag{2.8}$$

$$\boldsymbol{\varepsilon_{cell}} = \boldsymbol{\varepsilon_c} + \boldsymbol{\varepsilon_a} \tag{2.9}$$

Where the passive and active stresses would depend on the material behaviour ($\boldsymbol{\sigma_p} = f(\boldsymbol{\varepsilon_p})$ and $\boldsymbol{\sigma_c} = g(\boldsymbol{\varepsilon_a}) = h(\boldsymbol{\varepsilon_c})$).

For instance, considering both the actin and the passive as linear elastic materials, the equations would become:

$$\boldsymbol{\sigma_{cell}} = \boldsymbol{\sigma_c} + \boldsymbol{\sigma_p} = \boldsymbol{C_a}:\boldsymbol{\varepsilon_a} + \boldsymbol{C_p}:\boldsymbol{\varepsilon_p} = \boldsymbol{C_a}:(\boldsymbol{\varepsilon_{cell}} - \boldsymbol{\varepsilon_c}) + \boldsymbol{C_p}:\boldsymbol{\varepsilon_{cell}} \tag{2.10}$$

$$\boldsymbol{\varepsilon_{cell}} = \boldsymbol{\varepsilon_c} + \boldsymbol{\varepsilon_a} = \boldsymbol{\varepsilon_c} + \boldsymbol{C_a^{-1}}:\boldsymbol{\sigma_c} \tag{2.11}$$

where $\boldsymbol{C}$s are the material behavior tensors for the actin filaments and the passive components. In addition $\boldsymbol{\sigma_c}$ could be defined in several ways, for example (taking the expression from equation 2.4 (2)):

$$\boldsymbol{\sigma_c} = \begin{pmatrix} p_{max}/\varepsilon_{min}\,(\varepsilon_c^x - \varepsilon_{min}) & 0 & 0 \\ 0 & p_{max}/\varepsilon_{min}\,(\varepsilon_c^y - \varepsilon_{min}) & 0 \\ 0 & 0 & p_{max}/\varepsilon_{min}\,(\varepsilon_c^z - \varepsilon_{min}) \end{pmatrix} \tag{2.12}$$

2.2. Numerical implementation.

The model has been developed using ABAQUS 6.11® with user subroutines and based on the Finite Element Method (FEM). This allows the simulation of complex geometries, combining user-defined behaviours (the model) with Abaqus-library materials, obtaining high flexibility and adaptability to new experimental results that may alter the main hypothesis. Hence, the cell is modelled with double elements: one set corresponds to the passive side and the other one to the active contractile side. In this way, is not needed the development of specific and custom elements to reproduce the parallel behaviour of both components. Moreover, this fact simplifies the employment of several behaviour equations by changing the passive side of the model directly in the CAE module of the software.

Specifically, the cell active behaviour has been simulated as a thermal strain-dependent contraction, in parallel with the passive components simulated using different material definitions (elastic, hyperelastic, poroelastic). Different subroutines were necessary to run the model as described below:

Through the UEXTERNALDB subroutine the values of the controlled variables are initialized and the calculus process can be checked. With the URDFIL subroutine the values of the element identifier, node number and strain in every direction of all nodes involved in the cell contraction are obtained. Finally, using the UEXPAN subroutine, the expressions developed for cell contraction are implemented.

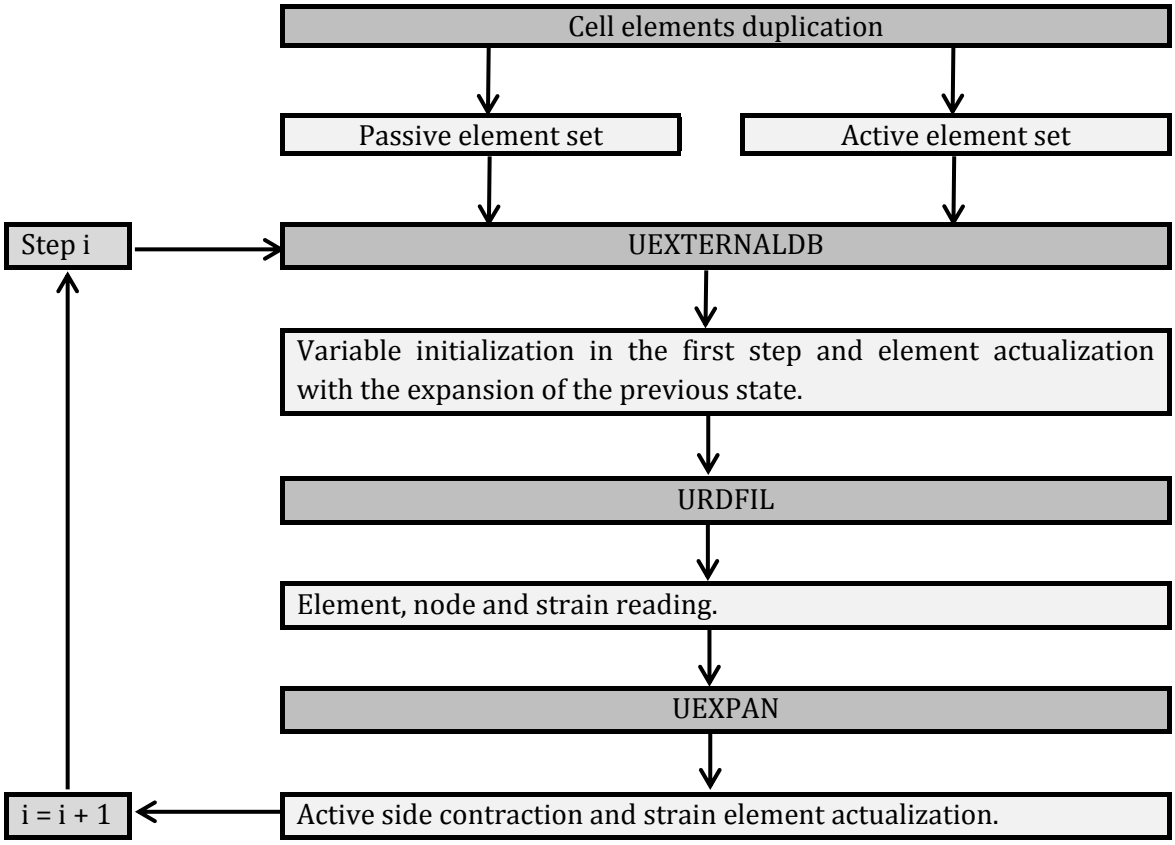

Figure 2.3. Computational algorithm.

The values used for each parameter of the contraction model are exposed in the Table 2.1. The parameters corresponding to the behavior of the substrate and the passive cell side will be detailed in the following sections according to each developed model.

Parameter	Description	Value	Reference
C_{act}	Actin elastic modulus	0.01 (MPa)	Schafer and Radmacher, 2005 [29]
ε_{min}	Minimum overlap of the AM fibres	-0.4	Moreo et al., 2008 [30]
ε_{max}	Maximum overlap of the AM fibres	0.4	Moreo et al., 2008 [30]
θ_{max}	Maximum stress exerted by the AM complex	2.5 (MPa)	Maskarinec et al., 2009 [31]

Table 2.1. Parameters used in the contraction model.

2.3. Behaviour of the passive component of the cytoskeleton.

The passive components of the cytoskeleton can be modelled according to different behaviour equations, depending on its complexity. Taking into account different behaviour laws allow determining which of them is more suitable for the cell contraction phenomenon. The two main approximations that will be considered are explained below.

a) Linear elastic.

Is the simplest model, defined by its elastic modulus and Poisson's coefficient. Experimental studies set these values in 1 – 75 kPa for elastic modulus with near incompressible behaviour, so Poisson's coefficient is near to 0.5 [29].

Nevertheless, the main limitation of this behaviour law is that it does not describe anything about the microstructure. The continuum mechanics replaces the contribution of the cytoskeletal discrete stress fibres with an averaged constitutive law that is applied at the whole cell.

b) Poroelastic.

The second possible approximation is the poroelastic model. In this model the following parameters must be defined: Logarithmic bulk modulus, Poisson's coefficient, stress limit, density, permeability and void ratio. The last one expresses the relationship between the void and solid part of the material by mean of the following expression:

$$e = \frac{V_v}{V_T - V_v} \tag{2.13}$$

where V_v is the void ratio and V_T is the total volumen. In this way, 1 corresponds to a totally void volume and 0 to a solid volume.

The values obtained for these parameters, according to experimental studies [32-33], can be observed in the table 2.3.

Parameter	K	G	σ_l	ρ	k	e
Value	0.001	15000	1000000	993.25	0.974	0.5

Table 2.2. Poroelastic model parameters. The units are: Dimensionless for the logarithmic bulk modulus *K*, Pa for the shear modulus *G*, Pa for the stress limit $\boldsymbol{\sigma_l}$, m/s for permeability *k* and kg/m^3 for density **ρ** at 37 ºC [32–33].

2.4. Model application to the Mitrossilis et al. experiment.

In order to experimentally determine forces exerted by cells in substrates of diverse stiffness, Mitrossilis et al. [1] carried out a study placing a C2.7 myoblast between two parallel microplates working as a microrheometer coated with fibronectin to improve cell adhesion, spread and contraction (Figure 2.4). The top plate was flexible and the lower plate could be considered as infinitely rigid. In this way, the cell pull down the top plate and the force, stiffness and displacement are correlated through:

$$F = K\delta \tag{2.14}$$

where K is the top plate stiffness and δ its deflection. Furthermore, the displacement of the top plate is equal to the shortening of the cell, thus the force rate is proportional to the shrinkage velocity.

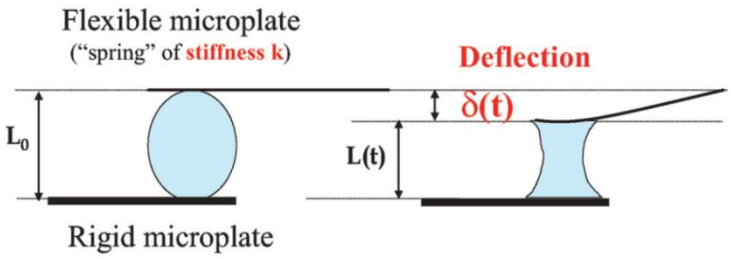

Figure 2.4. Force measurement method [1].

Force generation and the evolution in cell shape can be divided in three phases (Figure 2.5): First, the cell spreads and changes its form from convex to concave. In the second stage, the cell continue spreading, increasing the generated force during 10 minutes. Finally, the spreading stops and the force saturates.

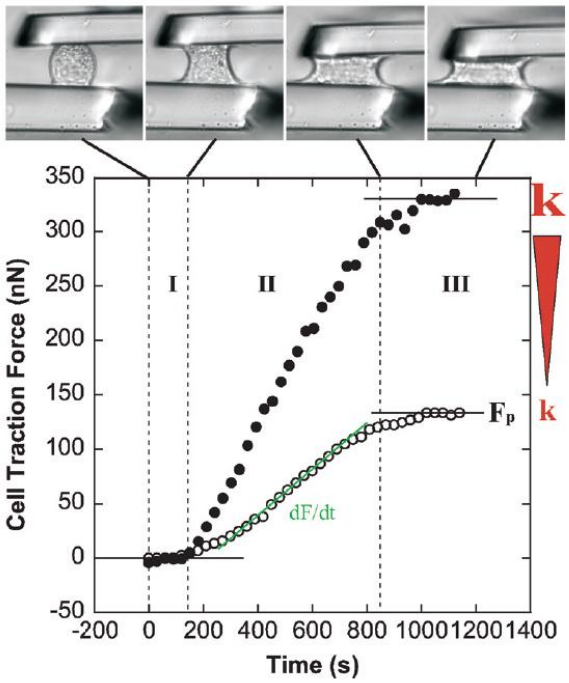

Figure 2.5. C2.7 Myoblast placed between two microplates. The evolution in cell shape along force generation can be divided in three main phases. The plateau force and the force rate increase while increasing the stiffness of the top plate. Two sets are represented: k = 21 nN/μm (open circles) and infinite stiffness (filled circles) [1].

It can be observed that the generated force is proportional to the stiffness of the flexible plate for rigidities lower than 60 nN/μm. For higher plate stiffness values, the force exerted saturates in ≈300 nN. These results are in agreement with experimental studies [35] that suggest that cells exert higher forces in stiffer substrates.

2.4.1. Finite Element Model description.

The developed model aims to accurately reproduce the experiment of Mitrossilis et al. [1]. In this way, the model comprises three main parts (Figure 2.6): The flexible top plate, modelled with shell elements, the cell, composed by hexahedrical elements, and the lower plate, modelled as a rigid solid.

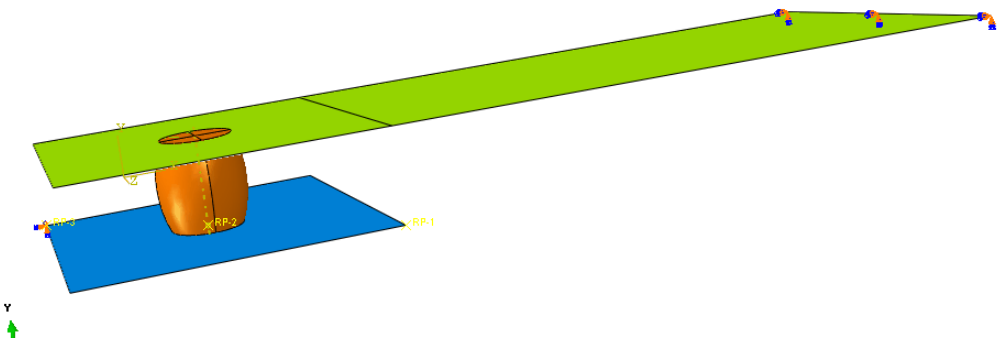

Figure 2.6. Developed model to reproduce the experimental study of Mitrossilis et al. [1]. Green: Flexible top plate. Orange: Cell. Blue: Rigid lower plate.

The cell properties for the active part are set according to the model described in section 2.2. Material formulation. The passive components follow the behaviours listed in section 2.4. With these settings and varying the elastic modulus of the top plate to achieve different values of stiffness, different cellular responses can be measured.

Since contact modelling is a challenging task, there were made successive approaches. In first instance, the cell shape was simplified to a cylinder with the interfaces totally attached to both plates. When the convergence was achieved for a wide variety of cantilever stiffnesses, friction coefficients were tested, aiming to a compromise value that allows cell spreading and enough attaching to the substrate. Following this, cell shape was changed to an oval shape, increasing the agreement between the Mitrossilis experiment and the computational model.

2.4.2. Results.

In this section the principal results of the model are shown. Further information about previous steps and calculus can be found in the Appendix I - Calculation report.

a) Linear elastic passive behaviour.

As a first approach, the cell was modelled with a linear elastic behaviour of the passive component with a cylinder like cell. During cell contraction, the shape changes, shrinking axially and changing its shape from a cylinder to a concave form as can be seen in figure 2.7.

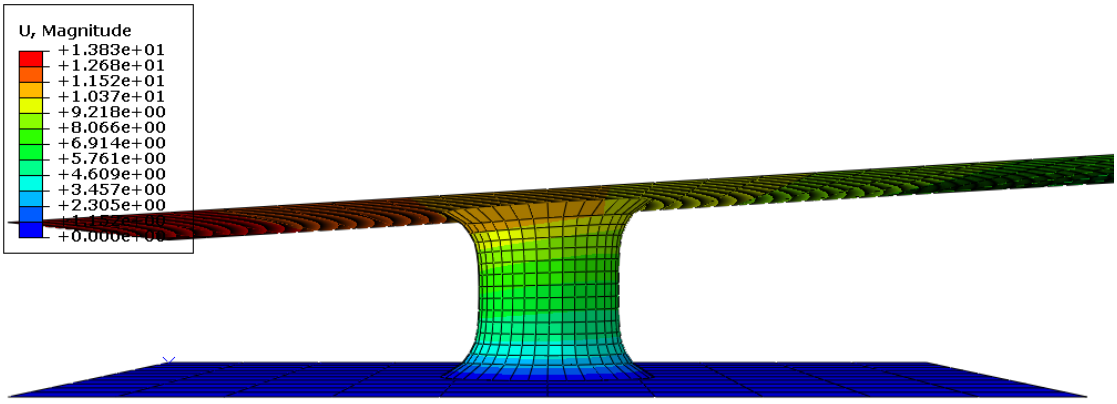

Figure 2.7. Cylinder like cell displacement with linear elastic passive behaviour. Flexible top plate stiffness: 15 nN/µm.

After several calculations with a wide variety of top plate stiffnesses it can be assumed that the axial strain of the cell is higher when the substrate is less stiff. Moreover, to higher stiffnesses, the axial displacement decreases to such degree that is smaller than the transversal displacement that leads the change in cell shape (Figure 2.8). This behaviour can be explained in a way that the cell feels its own stiffness and reacts consequently to its mechanical load.

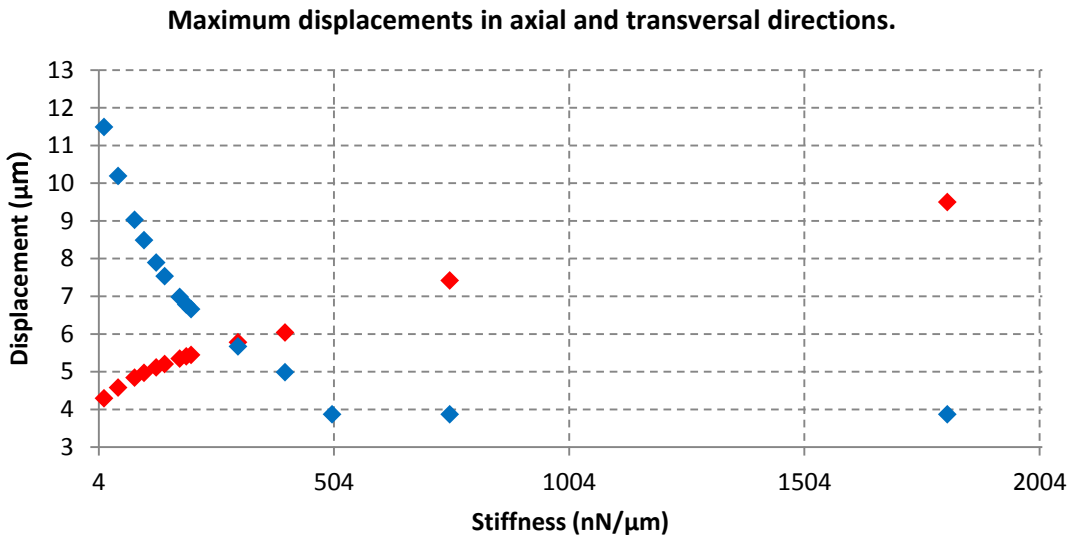

Figure 2.8. Maximum displacements obtained in the cell. Passive component characterized as linear elastic. Cylinder like cell. Blue: Axial displacement. Red: Transversal displacement.

The force exerted by the cell for the whole calculations are shown in figure 2.9.

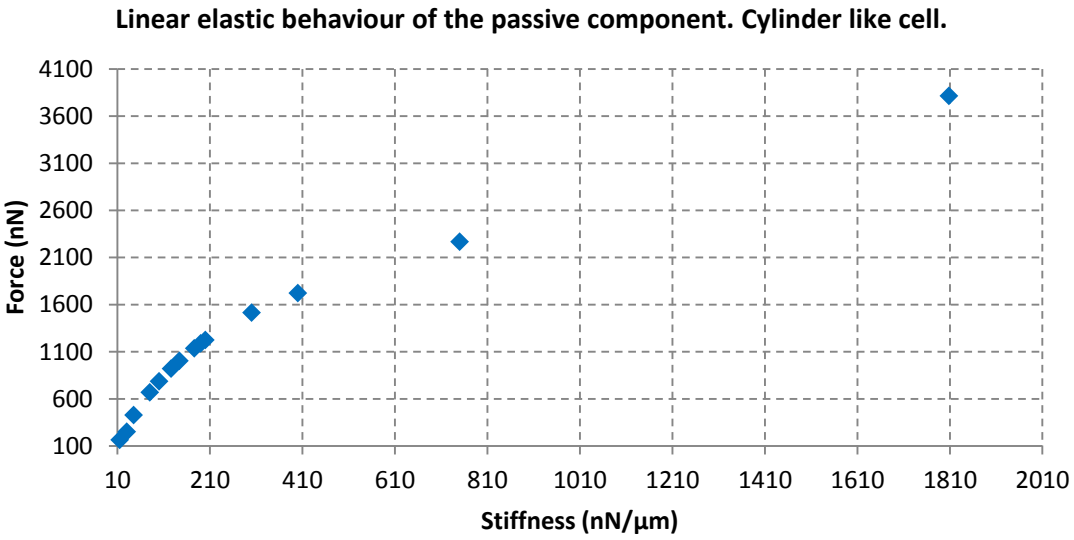

Figure 2.9. Force exerted by the cell for different stiffness values of the flexible top plate. Passive component characterized as linear elastic. Cylinder like cell.

In spite of the appropriate development of cell shape, there is not achieved a plateau force. Although it can be observed a change in the trend of the force exerted by the cell when it reaches 200 nN/µm, it is not enough to stabilize the force to a same value.

Therefore, an improvement in the model is needed. The first step is changing the cell shape to a barrel like cell in order to make a better match with the Mitrossilis et al. experiment [1].

Similarly to the previous case, the axial displacement decreases as the stiffness of the flexible top plate increases. Nonetheless, unlike the previous case, the axial displacement does not reach a maximum value for the studied values. The summary of these results can be seen in the figure 2.10.

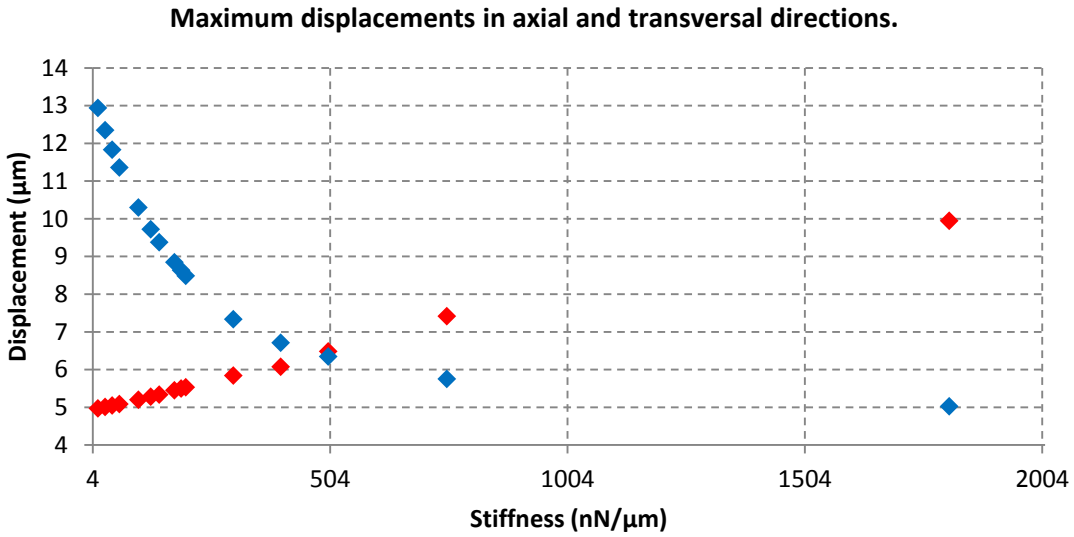

Figure 2.10. Maximum displacements obtained in the cell. Passive component characterized as linear elastic. Barrel like cell. Blue: Axial displacement. Red: Transversal displacement.

Eventually, using the same stiffness values and changing the cell shape, the forces exerted are shown in figure 2.11.

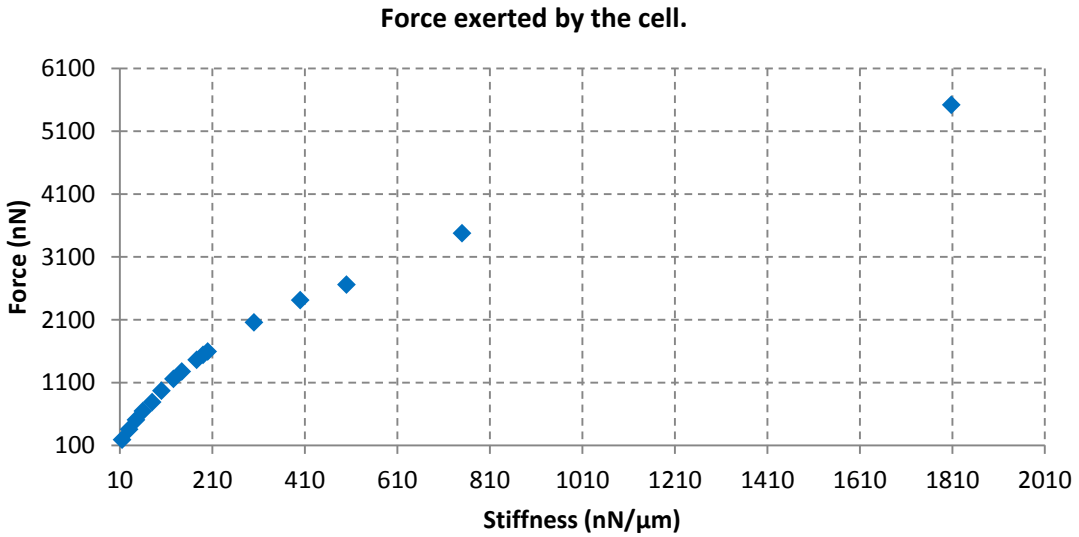

Figure 2.11. Force obtained for different stiffness values. Passive component characterized as linear elastic. Barrel like cell.

Even though the cell shape matches better with the actual experiment of Mitrossilis et al., the final cell shape as well as the exerted force does not agree with the expected behaviour.

b) Poroelastic passive behaviour.

Aiming to a better agreement with a real cell, it is proposed another passive behaviour based on a poroelastic model. Moreover, the contact behaviour is changed from a totally attached contact to a contact with friction, allowing the cell certain movement along the surface as can be seen in the edges of the cell in figure 2.12.

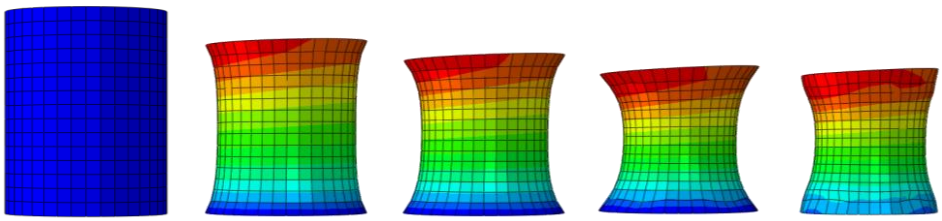

Figure 2.12. Evolution of cell shape along the contraction process with a cylinder like cell and poroelastic behaviour.

As previous cases, the axial displacement of the cell decreases as the stiffness of the flexible top plate increases. Nevertheless, the transversal displacement tends to stabilize, possibly due to the poroelastic behaviour of the passive side (Figure 2.13).

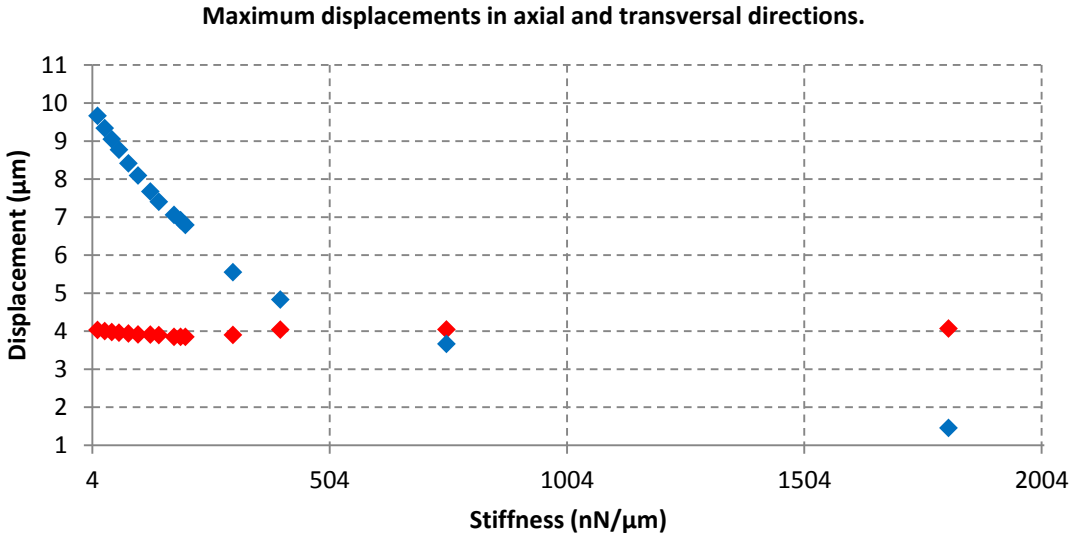

Figure 2.13. Maximum displacements obtained in the cell. Passive component characterized as poroelastic. Cylinder like cell. Blue: Axial displacement. Red: Transversal displacement.

The exerted forces for different top plate stiffnesses are shown in figure 2.14.

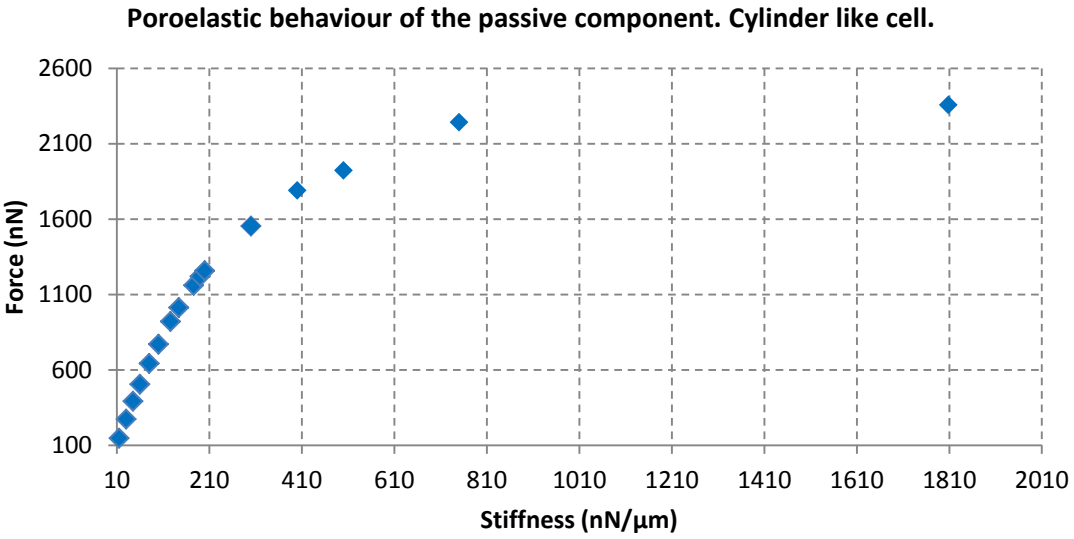

Figure 2.14. Force obtained for different stiffness values. Passive component characterized as poroelastic. Cylender like cell.

The main difference with the models with a linear elastic behaviour is that the cell reaches a plateau force between 2200 nN and 2400 nN once the stiffness of the flexible top plate is set to 750 nN/µm.

Nevertheless, although the force exerted by the cell behaves properly, reaching a maximum force after a specific stiffness, the evolution in cell shape does not agree with the observed in the experiment, in which the cell shrinks axially and spreads transversally.

2.5. Model application to real cell geometry.

2.5.1. Model description.

The studied cellular model is based on a breast cancer cell line MDA-MB-231 cultured using microfluidic devices. The cell was imaged under confocal microscopy and then reconstructed. Further explanation about cell reconstruction can be found in Appendix I – Calculation report. In the same way as the previous case, the cell is characterized with a passive and an active side.

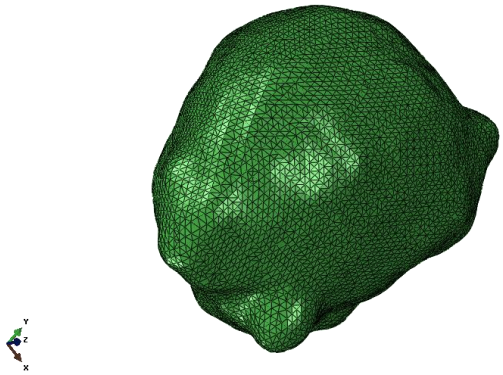

Figure 2.15. Cellular model obtained in the Centro de Investigación Médica Aplicada of Navarra.

2.5.2. Cell embedded in a substrate.

In this model, the cell is embedded in a cubic substrate of 194 μm side, characterized both as linear elastic as hyperelastic. The linear elastic model has an elastic modulus of 1 KPa and a Poisson's ratio of 0.49. For the hyperelastic consideration, the values are obtained via uniaxial test. The parameters are given in Appendix I – Calculation Report.

The passive component, according with the cell properties given by the CIMA, is characterized as linear elastic with an elastic modulus of 75 KPa and near-incompressible behaviour with a Poisson's ratio of 0.49.

The results showed in figure 2.16 show that cell strain differs depending on whether the cell is in a linear elastic substrate or in a hyperelastic substrate, producing not only a whole cell contraction but also an accentuation of the protrusion in the last case. This fact is in agreement with the probing role of the lamellipodia and filopodia in the mechanosensing mechanism.

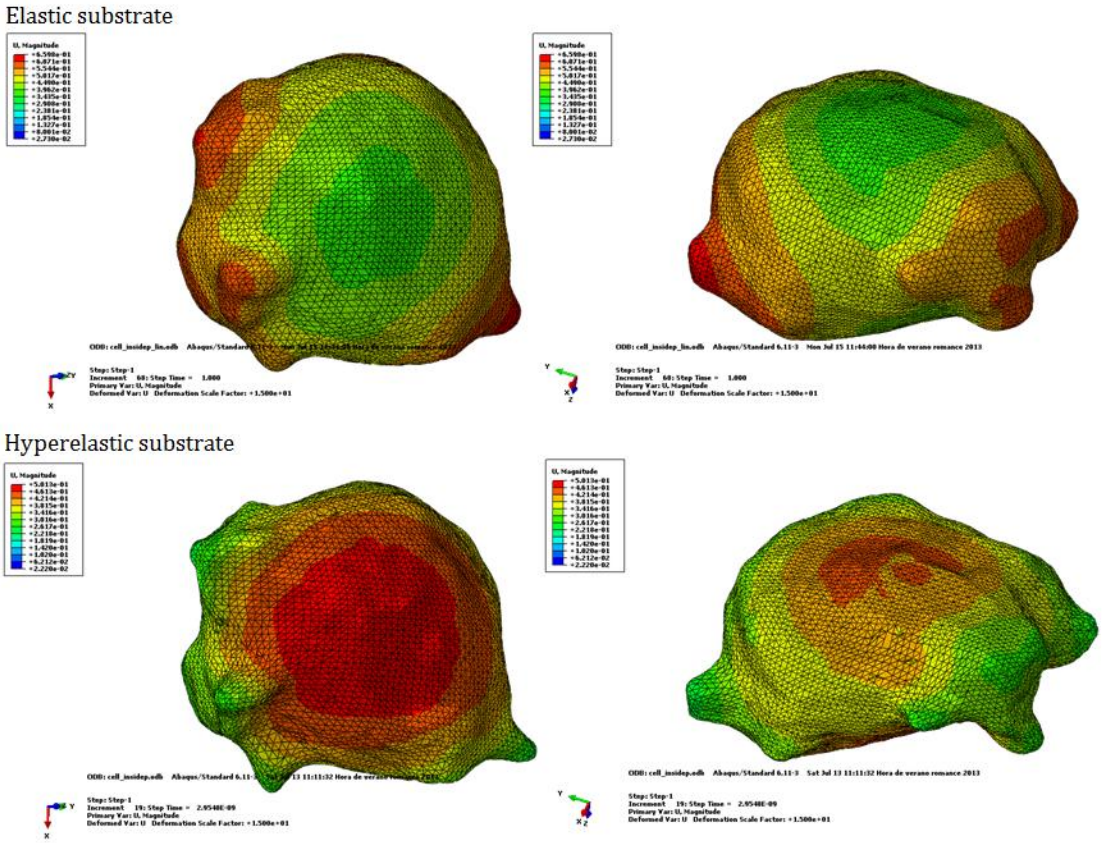

Figure 2.16. Rear view of the cell contraction obtained after the model application. Undeformed shape (translucent) and deformed shape (inside). Displacement displayed. It can be observed a cell contraction between 0.50 and 0.02 μm, with a protrusion accentuation. Scale factor: 15.

2.5.3. Simulating focal adhesions.

Since the cells are not totally attached to its substrate, the case developed above must be refined. As a first approach, the substrate is eliminated and it is replaced by springs as boundary conditions on the main protrusion of cell surface. Therefore, applying several stiffnesses to the springs, different kinds of the substrates can be modelled.

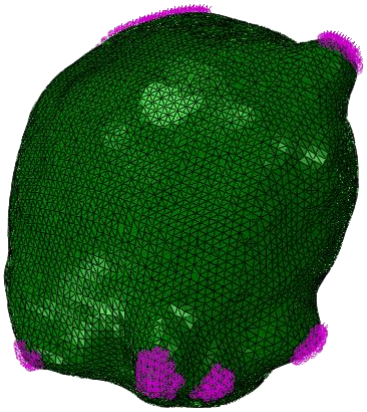

Figure 2.17. Cell (green) with focal adhesions placed on the protrusions (purple).

a) Cell without nucleus.

Firstly, the cell is studied without nucleus. As expected, the minimum cell displacement takes place in the focal adhesions whereas the cell body shrinks while it exerts force. Moreover, the stress distribution is uniform in the cell body, increasing in the adhesions.

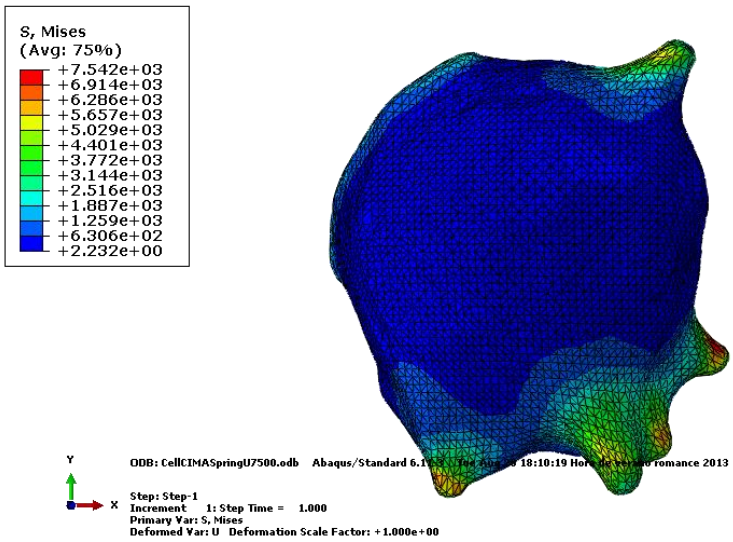

Figure 2.18. Stresses obtained with 7.5 nN/µm of focal adhesion stiffness.

After the analysis of the cell with several adhesion stiffnesses, the results of figure 2.19 are obtained. The cell displacement initially follows a linear behaviour until 50 nN/µm of focal adhesion stiffness. Then, the trend changes and the displacement reach a maximum value of 5.7 µm for the following focal adhesion stiffnesses. Furthermore, the displacement of the focal adhesions follows an exponential behaviour, reaching the minimum to stiffer substrates.

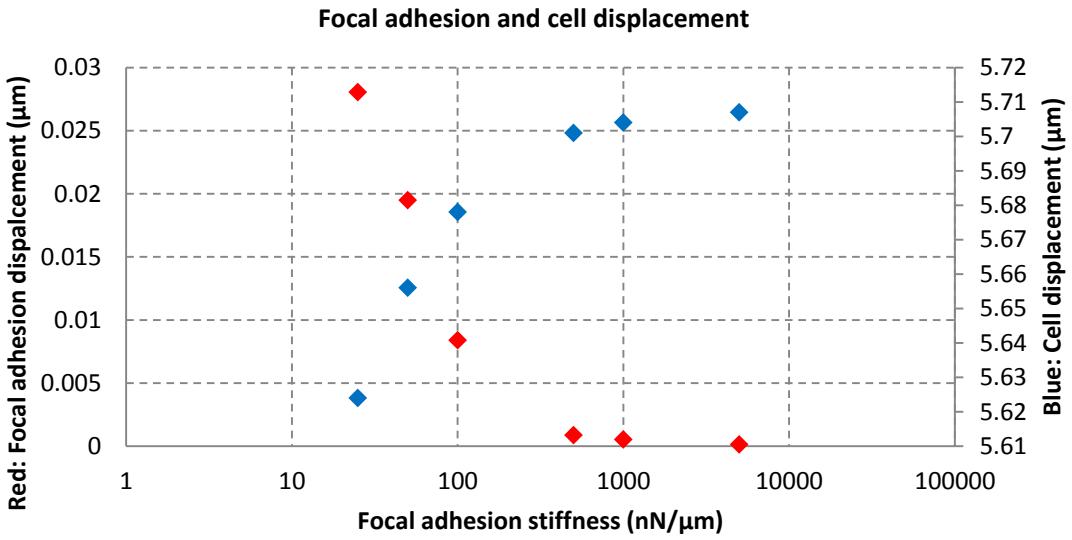

Figure 2.19. Focal adhesion displacement (red) and cell displacement (blue) depending on the stiffness of the substrate.

Abaqus® does not allow obtaining the reaction force in this kind of boundary conditions. Hence, considering that the stress is in relationship with the force exerted by the cell by mean of the maximum stress generated, the results in the figure 2.20 are obtained.

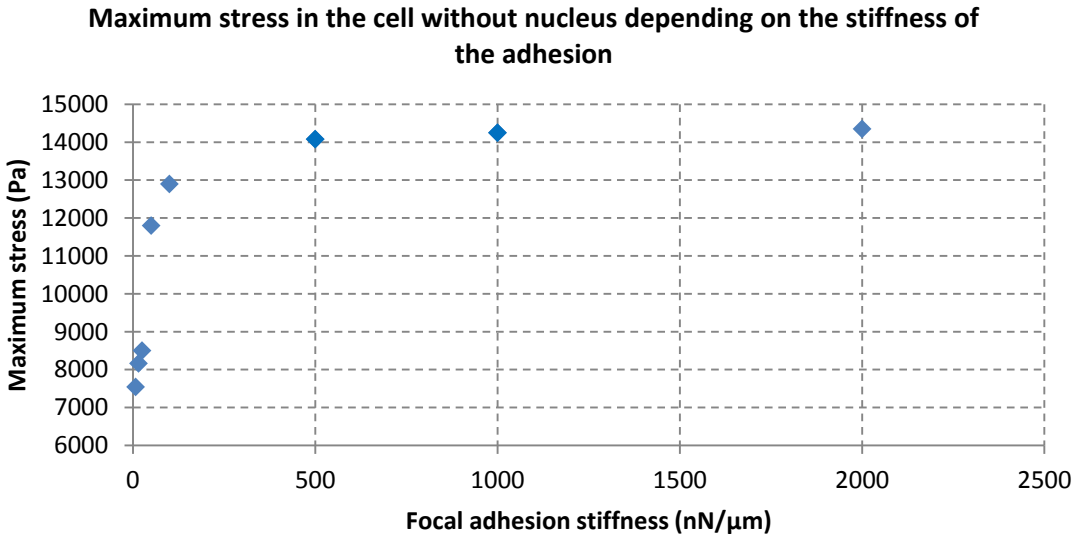

Figure 2.20. Maximum stress obtained within the cell without nucleus depending on the stiffness of the simulated adhesions.

The figure above shows that a plateau stress of 14.4 kPa is reached at a stiffness value of 500 nN/µm, where the cell cannot exert more force even though the substrate is stiffer.

b) Cell with nucleus.

Additionally, the cell is studied with a nucleus to study its influence in the process of cell contraction. Similarly to the previous case, the minimum cell displacement is obtained in the focal adhesions. It must be noted that when the nucleus is stiffer than the cytoskeleton, the contraction process exerts more force around the nucleus and generate stress in it (Figure 2.21).

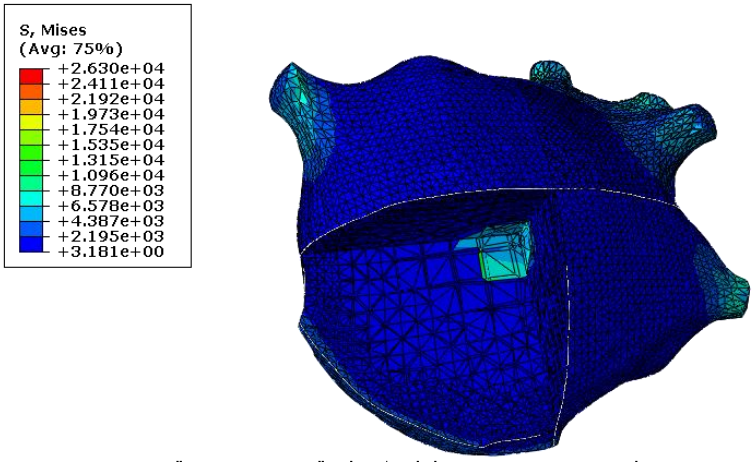

Figure 2.21. Stresses obtained with 100 nN/µm of focal adhesion stiffness. Inside the cell can be seen the nucleus stressed.

This process is also noticeable in the whole cell contraction because it shrinks more than the previous case, as it can be observed in figure 2.22.

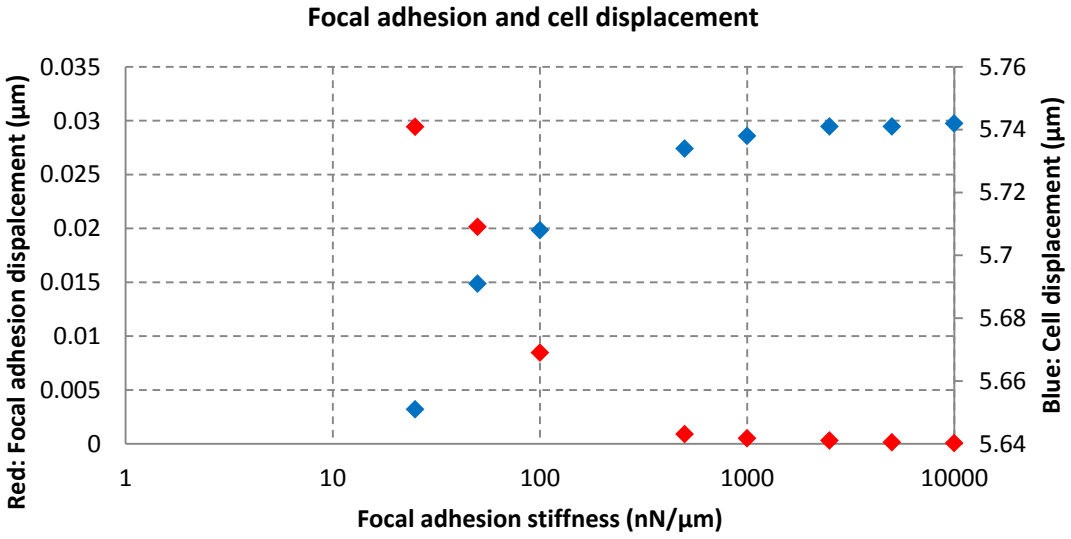

Figure 2.22. Focal adhesion displacement (red) and cell displacement (blue) depending on the stiffness of the substrate.

Nevertheless, the stress generated in the cell is similar to the previous case, reaching a maximum value around 14.5 kPa when the stiffness of the focal adhesion is set to 500 nN/ µm.

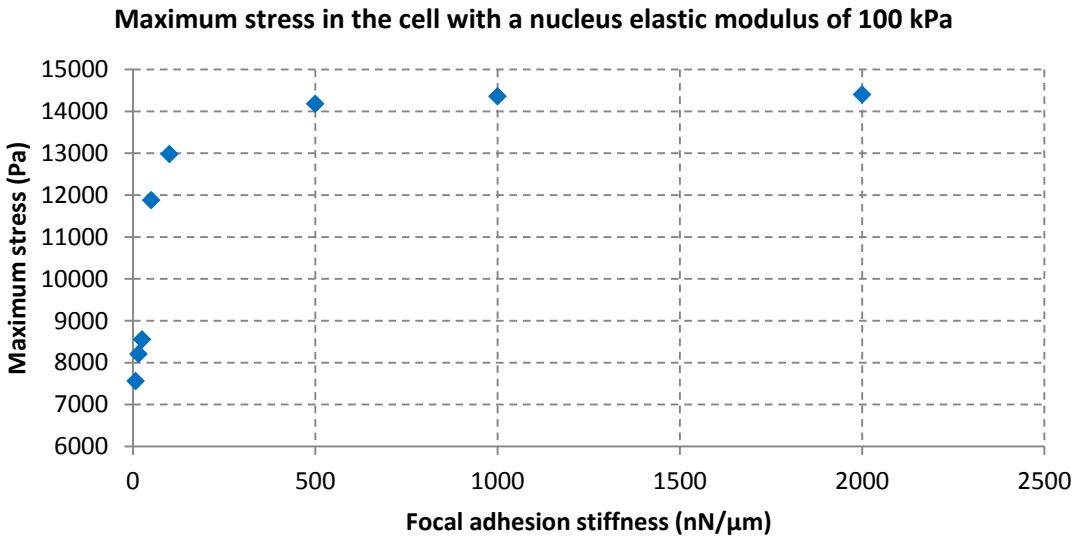

Figure 2.23. Maximum stress obtained within the cell with nucleus depending on the stiffness of the simulated adhesions. The elastic modulus of the nucleus is set to 100 kPa.

3. Conclusions.

Cell mechanosensing is a difficult and challenging field that must be approached carefully. Although the model did not work completely as expected, his work fixed the basis and guidelines for further research in this area.

3.1. Applying the model to the Mitrossilis et al. experiment.

The force exerted by the cell during its contraction, employing the linear elastic passive behaviour, does not agree with the results shown in the Mitrossilis et al. experiment [1], where the cell shrinks axially and spreads transversally, reaching a plateau force.

Notwithstanding, when the passive behaviour is modelled as poroelastic, a better agreement with the experiment is achieved. In other words, the final cell shape shows more similitude and a plateau force is achieved. There are two main reasons to approach this issue: The poroelastic model is closer to the behaviour of a real cell than the linear elastic one because it makes a simplification of the relationship between the cytoplasm and the organelles. Furthermore, the contact between the plates is changed to allow certain movement, which permits the cell exert force without the movement restriction imposed in the previous case. It must be noted that, even though the maximum force achieved differs from the experiment, the measurements of the model are an approximation and hence, differences in the force must be expected.

Additionally, although the final shape of the cell may seem adequate, the evolution during the cell contraction does not show any kind of transversal spreading that can be seen in the experiment. Nevertheless, a better agreement is achieved with the last model whereas with the linear elastic behaviour more transversal displacement was obtained.

Thanks to these conclusions it can be stated that, although the mechanosensing mechanism is leaded by the AM complex, there is another factor that takes part on the cell spreading. The first possible mechanism that must be taken into account in is the polymerization of actin filaments as the cell shrinks. Moreover, it must be studied the evolution of the cell volume while it shrinks because the preservation of the cell volume in the model could be a feasible solution to the main problem. Approaching this issue properly, it could be reached a better agreement with the cell behaviour because the cell could spread and, while spreading, exert more force on both plates thanks to a bigger surface, reaching a thinner final state similar to the experiment.

3.2. Applying the model to the cellular geometry obtained in the CIMA.

After applying the model to the real cell geometry can be obtained two main conclusions: As the substrate becomes stiffer, the contraction of the whole cell increases, in agreement with the exposed by some authors [34] who state that the cell migrates toward stiffer substrates because they can exert more forces. Additionally, the nucleus of the cell does not have influence on cell displacement but it has in the exerted force. In this way, the cell not only can sense the stiffness of its surrounding but also the stiffness of its own nucleus, applying force consequently. Therefore, for stiffer nucleus the cell exerts more force than for softer ones, where the main contribution of the nucleus is decreasing the ability of the cell to exert force.

4. Future work.

This model may be considered as the first step of a more complex model. However, although the AM complex works properly, it must be dealt the main problem stated before: the cell spreading must be included to a better agreement with the real behaviour.

Hence, it must be taken into account other passive behaviours, as well as looking for a way to make the cell shrink but also spread in the other directions maintaining the cell volume.

Once reached these objectives, this model could be included in a whole cell model to reproduce cell motility, the mechanosensing mechanism and even cell process guided by mechanical factors as, for example, cell differentiation.

5. Applications.

As previously exposed, this model can be useful as complement to a whole cell model to reproduce cell processes that includes mechanosensing. Increasing the knowledge in the mechanosensing mechanism it can be known how does it works and how can be controlled and thus, make accurate drugs.

Knowing the mechanosensing mechanism, the factors that have influence on this process can be controlled and treated if necessary. This fact is especially useful in diseases

as cancer, where the main problem is to understand how the cell migrates to another tissue. Although the cancerous cell travels through the blood vessels, first it must detach it from the tumorous mass. Therefore, aiming to these mechanisms, metastasis can be addressed and treated eliminating cell motility.

Moreover, the model can be used to model the wound healing as well as the recellularization of tissues employed in tissue engineering, increasing the knowledge in this field, increasing the accuracy of the parameters that must be controlled during this process and allowing the development of new techniques that can lead to new improvements in tissue engineering.

6. References.

[1] Mitrossilis, D. et al. 2009. Single-cell response to stiffness exhibits muscle-like behavior. *Proceedings of the National Academy of Sciences of the United States of America,* 106, 18243-18248.

[2] Bischofs, I. B. & Schwarz, U. S. 2003. Cell organization in soft media due to active mechanosensing. *Proceedings of the National Academy of Science of the United States of America,* 100, 9274-9279.

[3] Lin, S. –L., et al. 2009. Effects of compressive residual stress on the morphologic changes of fibroblasts. *Medical and biomedical Engineering and Computing,* 47, 1273-1279.

[4] Lo, C.M., Wang, H.B., Dembo, M. & Wang, Y.L. 2000. Cell movement is guided by the rigidity of the substrate. *Biophysical Journal,* 79, 144-152.

[5] Cukierman, E., Pankov, R., Stevens, D.R. & Yamada, K.M. 2001. Taking cell-matrix adhesions to the third dimension. *Science,* 294, 1708-1712.

[6] Schwarz, U.S. & Bischofs, I.B. 2005. Physical determinants of cell organization in soft media. *Medical Engineering & Physics,* 27, 763-772.

[7] Aznavoorian, S., et al. 1990. Signal transduction for chemotaxis and haptotaxis by matrix molecules in tumor cells. *Journal of Cell Biology,* 110, 1427-1438.

[8] Sanz-Herrera. J.A., Moreo, P., García-Aznar, J. M. & Doblaré, M. 2009. On the effect of substrate curvature on cell mechanics. *Biomaterials,* 30, 6674-6686.

[9] Dickinson, R. B. & Purich, D. L. 2002. Clamped-filament elongation model for actin-based motors. *Biophysical Journal,* 82, 605-617.

[10] Zhu, J. & Carlsson, A. E. 2006. Growth of attached actin filaments. *European Physical Journal E Soft Matter,* 21, 209-222.

[11] Mogilner, A. & Edelstein-Keshet, L. 2002. Regulation of actin dynamics in rapidly moving cells: a quantitative analysis. *Biophysical Journal,* 83, 1237-1258.

[12] Dawes, A.T., Bard Ermentrout, G., Cytrybaum, E. N. & Edelstein-Keshet. 2006. Actin filament branching and protrusion velocity in a simple 1D model of a motile cell. *Journal of Theoretical Biology,* 242, 265-279.

[13] Shemesh, T., Geiger, B., Bershadsky, A.D. & Kozlov, M. M. 2005. Focal adhesions as mechanosensors: A physical mechanism. *Proceedings of the National Academy of Sciences of the United States of America,* 102, 12383-12388.

[14] Novak, I. L., Slepchenko, B. M., Mogilner, A. & Loew, L. M. 2004. Cooperativity between cell contractility and adhesion. *Physical Review Letters,* 93.

[15] Ahmadi, A., Liverpool, T.B. & Marchetti, M. C. 2005. Nematic and polar order in active filament solutions. *Physical Review E Statistical, Nonlinear, and Soft Matter Physics,* 72, 060901.

[16] Kruse, K., Joanny, J. F., Julicher, F., Prost, J. & Sekimoto, K. 2005. Generic theory of active polar cells: a paradigm for cytoskeletal dynamics. *European Physical Journal E Soft Matter,* 16, 5-16.

[17] Zaman, M. H., Kamm, R.D., Matsudaira, P. & Lauffenburger, D. A. 2005. Computational model for cell migration in three-dimensional matrices. *Biophysical Journal,* 89, 1389-1397.

[18] Borau, C., Kamm, R. D. & García-Aznar, J.M. 2011. Mechano-sensing and cell migration: a 3D model approach. *Physical biology*, 8, 066008.

[19] Schluter, D.K., Ramis-Conde, I. & Chaplain, M. A. 2012. Computational modeling of single-cell migration: the leading role of extracellular matrix fibers. *Biophysical Journal,* 103, 1141-1151.

[20] Ouaknin, G. Y. & Bar-Yoseph, P. Z. 2009. Stochastic collective movement of cells and fingering morphology: no maverick cells. *Biophysical Journal,* 97, 1811-1821.

[21] Arciero, J. C., Mi, Q., Branca, M. F., Hackman, D. J. & Swigon, D. 2011. Continuum model of collective cell migration in wound healing and colony expansion. *Biophysical Journal,* 100, 535-543.

[22] Parkhurst, M. R. & Saltzman, W. M. 1992. Quantification of human neutrophil motility in three-dimensional collagen gels. Effect of collagen concentration. *Biophysical Journal,* 61, 306-315.

[23] Pettet, G. J., Please, C. P., Tindall, M. J. & McElwain, D. L. 2001. The migration of cells in multicell tumor spheroids. *Bulletin of Mathematical Biology,* 63, 231-257.

[24] Zaman, M. H. 2007. A multiscale probabilistic framework to model early steps in tumor metastasis. *Molecular Cell Biomechanics,* 4, 133-141.

[25] Zaman, M. H., Matsudaira, P. & Lauffenburger, D. A. 2007. Understanding effects of matrix protease and matrix organization on directional persistence and translational speed in three-dimensional cell migration. *Annals of Biomedical Engineering,* 35, 91-100.

[26] Buxboim, A., Ivanovska, I. L. & Discher, D. E. 2010. Matrix elasticity, cytoskeletal forces and physics of the nucleus: how deeply do cells 'feel' outside and in? *Journal of Cell Science,* 123, 297-308.

[27] Rassier, D. E., Macintosh, B. R. & Herzog, W. 1999. Length dependence of active force production in skeletal muscle. *Journal of Applied Physiology,* 86, 1445-1457.

[28] Huxley, A. F. 1957. Muscle structure and theories of contraction. *Progress in Biophysics and Biophysical Chemistry,* 7, 255-318.

[29] Schafer, A. & Radmacher, M. 2005. Influence of myosin II activity on stiffness of fibroblast cells. *Acta Biomaterialia,* 1, 273-280.

[30] Moreo, P., García-Aznar, J. M. & Doblaré, M. 2008. Modeling mechanosensing and its effect on the migration and proliferation of adherent cells. *Acta Biomaterialia,* 4, 613-621.

[31] Maskarinec, S. A., Franck, C., Tirrell, D. A. & Ravichandran, G. 2009. Quantifying cellular traction forces in three dimensions. *Proceedings of the National Academy of Sciences of the United States of America,* 106, 22108-22113.

[32] Moeendarbary, E. et al. 2013. The cytoplasm of living cells behaves as a poroelastic material. *Nature Materials,* 12, 253-261.

[33] Lo, C. M., Wang, H. B., Dembo, M. & Wang, Y. L. 2000. Cell movement is guided by the rigidity of the substrate. *Biophysical Journal,* 101, L33-5.